

Possible mechanism for superconductivity in doped SrTiO₃D. van der Marel ^{*}, F. Barantani, and C. W. Rischau*Department of Quantum Matter Physics, University of Geneva, 24 Quai Ernest-Ansermet, 1211 Geneva 4, Switzerland*

(Received 15 March 2019; revised manuscript received 14 July 2019; published 9 August 2019; corrected 28 October 2020)

The soft ferroelectric phonon in SrTiO₃ observed with optical spectroscopy has an extraordinarily strong spectral weight which is much stronger than expected in the limit of a perfectly ionic compound. This “charged phonon” effect in SrTiO₃ is caused by the close-to-covalent character of the Ti-O ionic bond and implies a strong coupling between the soft ferroelectric phonon and the interband transitions across the 3-eV gap of SrTiO₃. We demonstrate that this coupling leads, in addition to the charged phonon effect, to a pairing interaction involving the exchange of two transverse optical phonons. This process owes its relevance to the strong electron-phonon coupling and to the fact that the interaction mediated by a single transverse optical phonon vanishes at low electron density. We use the experimental soft phonon spectral weight to calculate the strength of the biphonon mediated pairing interaction in the electron-doped material and show that it is of the correct magnitude when compared to the experimental value of the superconducting critical temperature. Biphonon exchange is therefore an important pairing mechanism at low doping, and may be the key to understanding the occurrence of superconductivity in doped SrTiO₃ and other low electron density materials.

DOI: [10.1103/PhysRevResearch.1.013003](https://doi.org/10.1103/PhysRevResearch.1.013003)**I. INTRODUCTION**

The nature of superconductivity in SrTiO₃ [1–3] is exceptional for a number of reasons: Superconductivity occurs at extremely low carrier densities down to 10¹⁷ cm⁻³ [4,5], the material is close to a ferroelectric instability, and can be pushed into the ferroelectric state by appropriate Ca or ¹⁸O substitution [6–8], with a coexistence of superconductivity and a ferroelectric type symmetry breaking [9–11]. While the pairing mechanism is believed to have to do with electron-phonon coupling in some form [12–27], the question as to the exact nature of the electron-phonon interaction responsible for the pairing has not received a clear answer yet. As a result of the low carrier density, the Fermi temperature is low. Consequently, ϵ_F is of the same range or smaller than the phonon frequencies, placing the coupling to the longitudinal optic (LO) mode at 100 meV—to which the coupling is strongest—in the antiadiabatic limit [9,13,28,29]. Although it has been argued that the smallness of the Fermi surface has the consequence of drastically suppressing the available phase space for an electron-phonon interaction [16], it has been recently demonstrated that dominant single phonon exchange processes at low doping come from electronic states away from the Fermi surface [30]. Alternative pairing schemes include the exchange of intravalley phonons [12], two-phonon exchange [16], and longitudinal optical phonons [21]. However,

the LO-phonon mediated electron-electron interaction in the static limit is insufficient to describe superconductivity in strontium titanate, and an alternative approach has been explored based on the full dynamical dielectric function [19]. Much attention has been drawn by recent ideas on pairing mediated by the ferroelectric soft mode, and the effects on the pairing amplitude when the system approaches the quantum critical point of the ferroelectric order parameter. The quantum critical fluctuations of the ferroelectric order are often believed to be particularly good candidates for mediating a pairing interaction. However, one problem looms over this approach: The soft ferroelectric phonon (TO1) is a transverse optical mode. Processes whereby a *d* electron emits a TO phonon have a vanishing amplitude in the long-wavelength limit [27], which, due to the small Fermi momentum of these most dilute superconductors, is the relevant range. The corresponding longitudinal mode (LO1) has a frequency of about 20 meV, independent of temperature, and remains at this high energy through the phase transition (see Appendix A, Fig. 4). Another noteworthy feature is the fact that the electron-phonon coupling as described by the Frohlich model is negligible ($\alpha = 0.02$) for the LO1 phonon (see Appendix A, Fig. 4). This then raises the question whether there is any relevance at all of the soft ferroelectric modes in relation to the superconducting pairing mechanism.

II. SPECTRAL WEIGHT OF THE TO1 MODE

In the present paper an affirmative answer is provided to this question, but the nature of the interaction is unusual and the pairing process involves the exchange of two transverse polarized phonons as proposed by Ngai [16]. We begin by highlighting a striking feature [25,31] of the optical phonons of pristine SrTiO₃, namely, the fact that the TO1 mode has an

^{*}dirk.vandermarel@unige.ch

Published by the American Physical Society under the terms of the [Creative Commons Attribution 4.0 International license](https://creativecommons.org/licenses/by/4.0/). Further distribution of this work must maintain attribution to the author(s) and the published article's title, journal citation, and DOI.

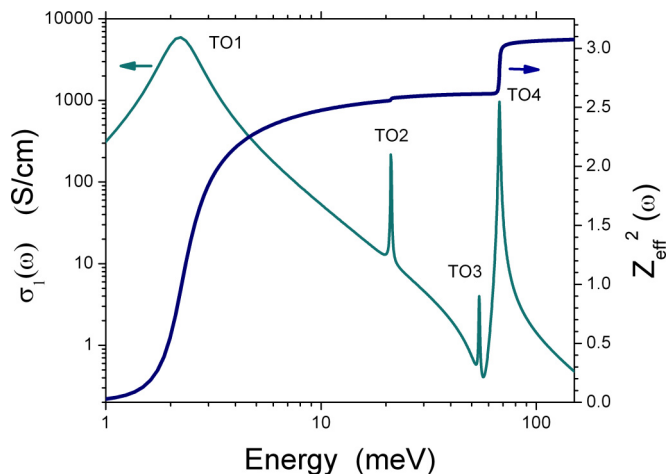


FIG. 1. Optical conductivity $\sigma_1(\omega)$ at 6 K (see Appendix A) and the sum-rule integral Z_{eff}^2 defined in Eq. (2), representing the transverse effective charge of the optical phonons of pristine SrTiO₃.

unusually strong oscillator strength. To make this quantitative we take a look at the integrated spectral weight of all phonons. The optical conductivity $\sigma_1(\omega)$ of the vibrational part of the optical spectrum satisfies the f -sum rule for the different species of ions in the compound, labeled by j ,

$$\int_0^{\Omega} \sigma_1(\omega') d\omega' = \sum_j \frac{\pi n_j q_j^2}{2m_j}, \quad (1)$$

where the parameters m_j , q_j , and n_j are the corresponding mass, charge, and volume densities and Ω is a suitably chosen cutoff above the upper limit of the vibrational part of the spectrum and below the lower limit of the interband transitions. In a purely ionic compound the charge q_j is given by the nominal valency. The ratio of both sides of the above expression,

$$Z_{\text{eff}}^2(\Omega) = \left[\sum_j \frac{\pi n_j q_j^2}{2m_j} \right]^{-1} \int_0^{\Omega} \sigma_1(\omega) d\omega, \quad (2)$$

then provides an effective charge which for a perfectly ionic compound is expected to be $Z_{\text{eff}}(\Omega) = 1$, as is indeed the case in simple salts such as MgO [32]. Figure 1 depicts $\sigma_1(\omega)$ of SrTiO₃ at 6 K determined experimentally from reflectivity measurements (Appendix A) and the corresponding partial integral $Z_{\text{eff}}^2(\omega)$. The latter amounts to a value of 3.1, implying that the effective charge is a factor 1.8 enhanced. Since the oxygen ions are by far the lightest ions and therefore are the dominant contributions to Eq. (1), one would be lead to conclude that the ionic charge is -3.5 instead of -2 , which makes absolutely no sense from a chemical perspective. For the case of SrTiO₃ this was answered in Ref. [31], namely, the “Ti-O ionic bond is on the verge of being covalent, leading to large charge transfers” [25]. In 1977, Rice analyzed this phenomenon in a different context of organic conductors, under the banner “charged phonons” [33], and the formalism has since then been applied to a number of different cases, including buckminsterfullerene [34], FeSi [35], and bilayer graphene [36].

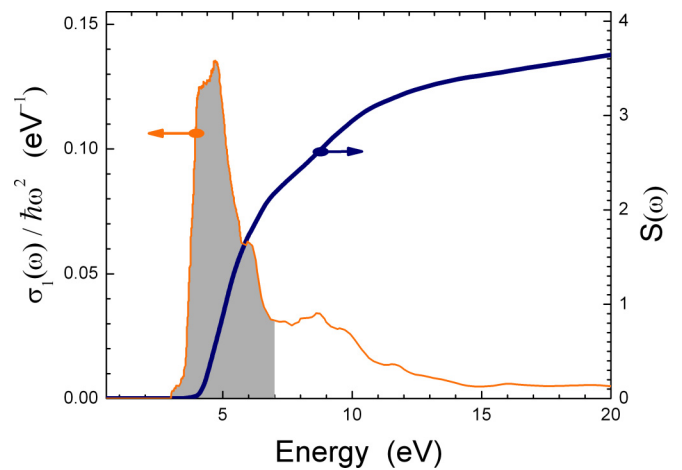


FIG. 2. Differential oscillator strength $\sigma(\omega)/\omega^2$ (orange). For $\hbar\omega < 5.7$ eV the dielectric function of Ref. [38] was digitized, and the optical conductivity data above 5.7 eV were digitized from Ref. [39]. The differential oscillator strength is the contribution of the optical conductivity per unit of energy to the static dielectric permeability $\epsilon(0)$. The dark blue curve represents the integrated oscillator strength taking 3 eV as the lower threshold. The gray area under the orange curve represents the energy range of O $2p$ to Ti $3d(t_{2g})$ transitions. The corresponding value of the oscillator strength of this transition can be read on the right-hand axis, corresponding to $S_e = 2.2$ eV.

In order to identify the main source of electron-phonon coupling we take advantage of the relation [see Appendix B, Eq. (B16)]

$$\epsilon(0) = 1 + \lim_{\omega \rightarrow \infty} S(\omega), \quad (3)$$

where

$$S(\omega) = 8 \int_0^{\omega} \frac{\sigma_1(\Omega)}{\Omega^2} d\Omega.$$

In Fig. 2 we show $\sigma_1(\omega)/\omega^2$ as well as the sum-rule integral $S(\omega)$ of this quantity for the electronic part of the spectrum, i.e., without the phonon contribution of Fig. 1. From the early band-structure calculations using the linear combination of atomic orbitals (LCAO) method, it is possible to identify the range from 3 to 7 eV with transitions from the occupied O $2p$ states to the empty Ti $3d(t_{2g})$ bands [37]. The latter bands, which are empty in pristine SrTiO₃, become populated when electron doping the material, and the electrons in these bands are those which exhibit superconductivity. The experimental differential oscillator strength shown in Fig. 2 makes abundantly clear that the lion’s share of the static polarizability originates from the mixing of O $2p$ and Ti $3d(t_{2g})$ character, and that the corresponding oscillator strength is $S_e = 2.2$. We can combine this with our knowledge of Z_{eff}^2 to obtain the value of the classical (spring) coupling constant γ , the electronic and vibrational length scales a_e [Eq. (B17)] and a_n [Eq. (B28)], and the transverse electron-phonon coupling constant g [Eq. (B30)]. The resulting values of these parameters are given in Table I.

TABLE I. List of the experimental quantities (left) and derived theoretical quantities (right).

Quantity	Value	Units	Quantity	Value	Units
Z_{eff}^2	3.1	^a	\tilde{m}_e	0.84	m_e
$N_{e,p}$	2.0	^a	a_e	9.5×10^{-9}	cm
V	5.95×10^{-23}	cm ³ [2]	a_n	1.0×10^{-9}	cm
$\hbar\omega_n$	12	meV ^b	γ	9.3×10^4	g/s ²
$\hbar\omega_e$	5.0	eV ^a	g	0.57	eV
S_e	2.2	^a	Γ	66	meV
D_F^*	≤ 0.80	eV ⁻¹ [18]	$\lambda_{2\text{ph}}$	≤ 0.28	
T_c	≤ 400	mK [1]	λ_{expt}	≤ 0.15	

^aPresent work.^bEstimated from the $\omega(q)$ dispersion of TO1 reported in Ref. [42].

III. TWO-PHONON EXCHANGE AND SUPERCONDUCTIVITY

Equipped with these parameters we are now in a position to analyze further consequences of the electron-phonon coupling described by the Hamiltonian [see Appendix B, Eq. (B29)]

$$\hat{H} = \epsilon_p \hat{p}^\dagger \hat{p} + \epsilon_d \hat{d}^\dagger \hat{d} + \hbar\omega_n \left(\frac{1}{2} + \hat{a}^\dagger \hat{a} \right) - g(\hat{d}^\dagger \hat{p} + \hat{p}^\dagger \hat{d})(\hat{a}^\dagger + \hat{a}), \quad (4)$$

where the label d refers to the central titanium $3d_{xy}$ state, and p refers to the even superposition of two π -bonded oxygen $2p_y$ states to the left and right of the central titanium $3d_{xy}$ state. The energy separation of these two states is $\hbar\omega_e = \epsilon_d - \epsilon_p$, the corresponding electron creation and annihilation operators are \hat{d}^\dagger , \hat{p}^\dagger , \hat{d} , and \hat{p} , and \hat{a}^\dagger (\hat{a}) creates (annihilates) a vibrational quantum. The momentum dependence is provided in Appendix B 1. For the present purpose we will just work out the consequences in the local model described by Eq. (4). The first important point to note is the fact that the emission or absorption of a phonon implies a change of parity of the electronic wave function. For bands close to the Brillouin-zone center this implies that the electron has to switch necessarily from one band to another. The main players are the occupied O $2p$ bands and the empty Ti $3d$ bands, the latter ones of t_{2g} character immediately above the insulator gap (3 eV) and the e_g states at 2.5 eV higher energy. The implication is that in the limit $k_F \rightarrow 0$, a process whereby a single TO1 phonon is exchanged between two conduction electrons has zero amplitude. The next available process involves the exchange of two phonons. We consider first a state with a single d electron doped into the insulator. The electron-phonon interaction in Eq. (4) generates on top of this a virtual electronic excitation and a phonon, together having an energy $\omega_e + \omega_n$, which decays into a state with again a single d electron and two phonons. In second-order perturbation theory the corresponding scattering amplitude is

$$\Gamma \approx -\frac{g^2}{\hbar\omega_e}, \quad (5)$$

where we used that $\omega_n \ll \omega_e$. The value is reported in Table I. The two emitted phonons can be reabsorbed by a second d electron in a similar process, causing the two d electrons to interact by virtual exchange of two optical phonons. Following

the standard treatment of BCS theory we obtain for the product of pairing interaction and density of states D_F^* at ϵ_F ,

$$\lambda_{2\text{ph}} = 2D_F^* \frac{\Gamma^2}{2\hbar\omega_n}. \quad (6)$$

where the factor 2 in front of the expression accounts for the two possible permutations of the biphonon exchange [40] and the factor 2 in the denominator accounts for the fact that the interaction is mediated by a pair of phonons. Since in a lattice environment the phonon frequency disperses as a function of momentum, the factor $1/(2\omega_n)$ on the right-hand side should be replaced by the momentum average of $1/(\omega_q + \omega_{q'})$, for which we obtain [41] $2\hbar\omega_n = 24$ meV. Combining all experimental factors used to evaluate g , Γ , and $\lambda_{2\text{ph}}$ we can write Eq. (6) as

$$\lambda_{2\text{ph}} = \frac{\hbar(8\pi)^2 n_{e,p}^2 g_e^4 (Z_{\text{eff}}^2 - 1)^4 D_F^*}{S_e^2 m_n^2 \omega_n^3}. \quad (7)$$

The thus obtained value for the electron-electron coupling constant is $\lambda_{2\text{ph}} = 0.28$. This falls well inside the range of values of the coupling parameter estimated from T_c data ($0.1 < \lambda_{\text{expt}} < 0.2$) and transport ($0.1 < \lambda_{\text{expt}} < 0.4$) for carrier concentrations from 10^{19} to 10^{20} cm⁻³ (see Fig. 8 of Ref. [18]). The close value of $\lambda_{2\text{ph}}$ to λ_{expt} is encouraging and shows that Ngai's model [16] of the exchange of two optical phonons could be relevant for superconductivity in SrTiO₃.

IV. DISCUSSION AND OUTLOOK

We started out by analyzing the observed, strong, charged phonon effect in pristine SrTiO₃, and proceeded to extract an electron-phonon coupling constant relevant in biphonon pairing processes. Usually when the charged phonon effect is observed, the electronic oscillator and the phonon oscillator are much closer in energy, and in fact often overlap, leading to interesting resonance behavior and Fano asymmetries. In the present case the vibrational and electronic energy scales are separated by two orders of magnitude, making the case for SrTiO₃ quite exceptional in that the large observed Z_{eff} implies that the charged phonon interaction is abnormally strong. These materials are close to a ferroelectric instability, such an instability requires the harmonic potential to switch sign near the phase transition, the ferroelectric displacement is exactly what is driving the charged phonon effect, and it is difficult to identify a pairing mechanism of the doped superconducting materials. From an intellectual point of view it would be satisfying if a common factor could be identified which is responsible for all of those phenomena. The model proposed in the present paper fits this description, and solves the conundrum of the electron coupling to the soft ferroelectric modes despite the fact that these modes are transverse polarized. The softening of the mode brings along the difficulty that any anharmonicity in the potential of the vibrational coordinate becomes particularly pronounced (e.g., a mexican hat shape) and the vibrational frequency becomes imaginary [43]. This immediately leads to the problem that parameters such as γ and a_n lose their meaning, at least in the long-wavelength limit where the softening takes place. A treatment of the biphonon exchange processes including the aforementioned features

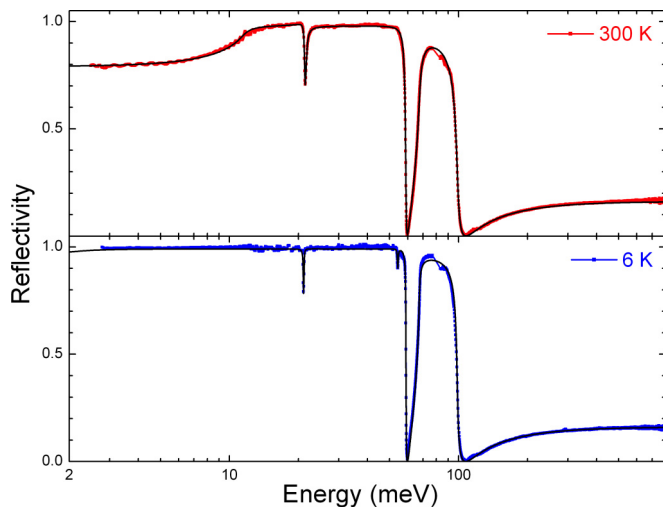


FIG. 3. Experimental reflectivity data of pristine SrTiO₃ at room temperature and 6 K and fits (solid black curves) using Drude-Lorentz oscillators with Fano-shape asymmetry.

should be the subject of future studies. The current state of affairs provides a motivation to undertake further theoretical and experimental studies. At the present stage a number of falsifiable consequences can already be stated. In particular, the soft two-phonon processes, corresponding to a broad continuum of the biphonon energies (about 25–30 meV), should show up in tunneling and photoemission spectra, with an electron-phonon coupling constant $g \sim 0.6$ eV. Another consequence is that the pulsed optical excitation of the pd electron-hole excitations using a laser operating between 3 and 7 eV should lead to a pronounced coherent excitation of the soft ferroelectric modes. This method provides an alternative scheme to measure the coupling constant g . Finally, we note that, while doped SrTiO₃ presents a confluence of properties including the charged phonon effect which allows one to obtain from optical experiments the coupling strength of the conduction electrons to two-phonon processes, similar couplings may play a role in other low-density superconductors.

ACKNOWLEDGMENTS

This project was supported by the Swiss National Science Foundation (Project No. 200020-179157). D.v.d.M. acknowledges insightful discussions with Dung-Hai Lee, Dimitri Abanin, Nicola Spaldin, Alexander Balatsky, Jonathan Ruhman, Tom Devereaux, Jan Zaanen, and Dmitrii Maslov.

APPENDIX A: EXPERIMENTAL OPTICAL CONDUCTIVITY DATA, ENERGY LOSS FUNCTION, AND ELECTRON-PHONON COUPLING FUNCTION

Figure 3 shows the experimental reflectivity spectra of SrTiO₃ at room temperature and 6 K. The data have been fitted with a multis oscillator function. The complex dielectric function obtained by this procedure is a smooth function suitable for calculating the derivative in Eq. (A1). Note that at the lowest temperatures the frequency of the TO1 mode

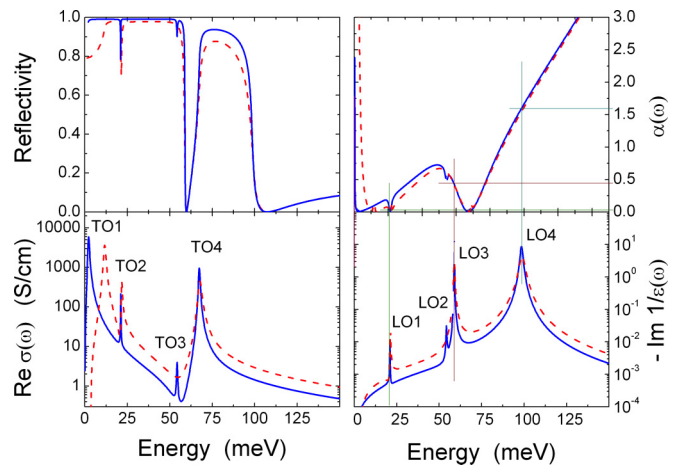


FIG. 4. Reflectivity (top left), optical conductivity (bottom left), loss function (bottom right), and coupling function (top right) of pristine SrTiO₃ at room temperature (red dashed) and 6 K (solid blue) curve. The peaks of the optical conductivity (loss function) correspond to the TO (LO) modes. To allow for $\alpha(\omega)$ to be smooth despite the frequency derivative in the denominator, a Lorentz parametrization of the optical spectrum was used. The vertical and horizontal lines in the right-hand panels graphically represent the α coefficients corresponding to each of the longitudinal phonons.

ω_1 falls below the window of observation of the reflectivity experiments (i.e., below 2.5 meV in Fig. 5). While the multis oscillator fit is not expected to accurately reproduce $\sigma(\omega)$ in the range where there are no experimental data, the spectral weight S_1 of the TO1 mode shows up as a negative contribution to $\text{Im } \sigma(\omega)$ at higher frequencies proportional to $-S_1 \omega_1^2 / \omega$ and can be obtained reliably by this method. The corresponding optical conductivity shown together with the loss function in Fig. 4 confirms the results reported in Refs. [44–46]. The peaks in the optical conductivity coincide with the TO modes, and the peaks in the loss function with the LO modes. The top right panel shows the electron-phonon coupling constants calculated using Eq. (A1). The first point to notice is the strong difference in temperature dependence of TO and LO modes. Whereas the TO1 mode is strongly temperature dependent and approaches zero energy at zero temperature, all LO modes including the one lowest in energy (LO1) are essentially temperature independent.

The second observation is that the electron-phonon coupling to the LO1 mode is negligible as compared to the other two. This is seen from the coupling constants described by Toyozawa’s multiphonon generalization of the Fröhlich model [47,48],

$$\alpha_j = \sqrt{\frac{2m_b}{\hbar^3 \omega_{L,j}^3}} \frac{q_e^2}{[\partial \epsilon / \partial \omega]_{L,j}}. \quad (\text{A1})$$

The values of α can be readily read off from the top right panel of Fig. 4, and correspond to those that have been used by Devereaux *et al.* [28] to calculate the midinfrared band of electron-doped SrTiO₃. The good agreement of those calculations with the data of Ref. [46] demonstrates the validity of the α parameters obtained with the method of Fröhlich.

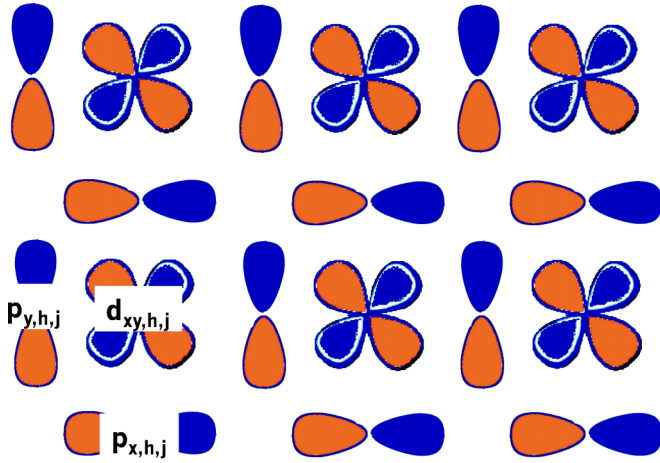


FIG. 5. While SrTiO₃ is a three-dimensional crystal, the relevant valence states are built up from oxygen 2*p* and titanium 3*d*_{xy} orbitals as sketched in this figure. If we label the horizontal and vertical axis as *x* and *y*, one should imagine that this structure is repeated along the *z* axis of the simple cubic structure. The corresponding bands are degenerate with, and orthogonal to, the bands comprising 3*d*_{yz} and 3*d*_{zx} with corresponding oxygen 2*p* orbitals.

We should therefore take seriously that the electron-phonon coupling to the lowest-energy longitudinal mode is very small, and most likely insignificant in the context of the mechanism for superconductivity.

APPENDIX B: DETAILS OF THE FORMALISM

Bringing elements together from scattered texts comes with the risk of missing a factor of π or 1/2 here and there. Since at the end of the day we need to compute numbers that can be compared with experiments, we will derive the charged-phonon formalism and the resulting biphonon pairing mechanism from scratch.

1. Momentum dependence of the band structure and electron-phonon interaction

The relevant orbitals are depicted in Fig. 5. The tight-binding Hamiltonian with nearest-neighbor hopping corresponding to the orbitals in a single plane is

$$\begin{aligned} \hat{H} = & \sum_{h,j} (\epsilon_d \hat{d}_{xy,h,j}^\dagger \hat{d}_{xy,h,j} + \epsilon_p \hat{p}_{x,h,j}^\dagger \hat{p}_{x,h,j} + \epsilon_p \hat{p}_{y,h,j}^\dagger \hat{p}_{y,h,j}) \\ & + t_{pd} \sum_{h,j} (\hat{p}_{y,h,j}^\dagger \hat{d}_{xy,h,j} + \hat{p}_{x,h,j}^\dagger \hat{d}_{xy,h,j}) + \text{H.c.} \\ & - t_{pd} \sum_{h,j} (\hat{d}_{xy,h,j}^\dagger \hat{p}_{y,h+1,j} + \hat{d}_{xy,h,j}^\dagger \hat{p}_{x,h,j+1}) - \text{H.c.} \end{aligned} \quad (\text{B1})$$

Diagonalization is straightforward and gives

$$\hat{H} = \sum_{j=1}^3 \sum_k \epsilon_{k,j} \hat{c}_{k,j}^\dagger \hat{c}_{k,j}, \quad (\text{B2})$$

where the three bands are described by the following energy-momentum dispersions,

$$\begin{aligned} \epsilon_{k,1} &= \frac{\epsilon_d + \epsilon_p}{2} - \sqrt{\frac{(\epsilon_d - \epsilon_p)^2}{4} + \tau_k^2}, \\ \epsilon_{k,2} &= \epsilon_p, \\ \epsilon_{k,3} &= \frac{\epsilon_d + \epsilon_p}{2} + \sqrt{\frac{(\epsilon_d - \epsilon_p)^2}{4} + \tau_k^2}, \\ \tau_k &= 2t_{pd} \sqrt{\sin^2\left(\frac{k_x a}{2}\right) + \sin^2\left(\frac{k_y a}{2}\right)}. \end{aligned} \quad (\text{B3})$$

The natural cause of the electron-phonon interaction in this paper is the Peierls interaction, the modulation of the bond strength due to the lattice displacement, which leads to the following expression,

$$\begin{aligned} \hat{H}_c = & -g' \sum_{h,j} \hat{d}_{h,j}^\dagger (\hat{p}_{y,h,j} + \hat{p}_{y,h+1,j}) (\hat{a}_{x,h,j}^\dagger + \hat{a}_{x,h,j}) \\ & - g' \sum_{h,j} \hat{d}_{h,j}^\dagger (\hat{p}_{x,h,j} + \hat{p}_{x,h+1,j}) (\hat{a}_{y,h,j}^\dagger + \hat{a}_{y,h,j}) - \text{H.c.} \end{aligned} \quad (\text{B4})$$

Fourier transformation gives for the special case of phonons traveling along q_y ($q_x = 0$),

$$\begin{aligned} \hat{H}_c = & -2g' \sum_{\vec{k}, q_y} \cos\left(\frac{k_x a}{2}\right) [\hat{d}_{\vec{k}}^\dagger \hat{p}_{y, \vec{k}+\vec{q}} + \hat{p}_{y, \vec{k}-\vec{q}}^\dagger \hat{d}_{\vec{k}}] [\hat{a}_{x, \vec{q}}^\dagger + \hat{a}_{x, -\vec{q}}] \\ & - 2g' \sum_{\vec{k}, q_y} \cos\left(\frac{k_y a + q_y a}{2}\right) \hat{d}_{\vec{k}}^\dagger \hat{p}_{x, \vec{k}+\vec{q}} [\hat{a}_{y, \vec{q}}^\dagger + \hat{a}_{y, -\vec{q}}] \\ & - 2g' \sum_{\vec{k}, q_y} \cos\left(\frac{k_y a - q_y a}{2}\right) \hat{p}_{x, \vec{k}-\vec{q}}^\dagger \hat{d}_{\vec{k}} [\hat{a}_{y, \vec{q}}^\dagger + \hat{a}_{y, -\vec{q}}]. \end{aligned} \quad (\text{B5})$$

The operators $\hat{d}_{\vec{k}}^\dagger$, $\hat{p}_{x, \vec{k}}$, and $\hat{p}_{y, \vec{k}}$ can be decomposed in the band-eigenstate operators $\hat{c}_{\vec{k}, j}^\dagger$. For the present purpose it suffices to point out that the two main players are bands $j = 2$ and $j = 3$. The character of band 2 is a pure nonbonding *p* band. In the limit of large ω_e/t_{pd} the character of band $j = 3$ becomes purely Ti 3*d*. For the purpose of the present paper, where the coupling constants are obtained from experimental data, it is not necessary to work out these equations in more detail. It is, however, interesting and of potential importance to notice that the Peierls coupling provides in addition to the charged phonon term (the first line of the equation) also a coupling to longitudinal phonons (second and third lines of the equation).

2. Two-level model of the charged phonon effect

From here on we consider a simplified version of the band structure, ignoring the energy-momentum dispersion of the bands, comprising for each lattice site of volume *V* an occupied level corresponding band $j = 2$ of the previous section and an empty state corresponding to band $j = 3$, which we will label *p* and *d* for brevity. Both hybrid states have their center of mass at the same (Ti⁴⁺) atomic site. The relevant electronic levels are depicted in Fig. 5. For two O²⁻ ions

adjacent to Ti^{4+} ions with the three ions aligned along the x axis this implies that we consider the even combination of the two O p_y orbitals with its center of mass at the Ti $3d_{xy}$ state. For an electric field polarized along the x direction, the p - d transition is dipole allowed. This system is described by the Hamiltonian

$$\hat{H}_e = \epsilon_p \hat{p}^\dagger \hat{p} + \epsilon_d \hat{d}^\dagger \hat{d}. \quad (\text{B6})$$

The position operator follows from the consideration that p and d have the same center of mass. A linear combination $u|p\rangle + v|d\rangle$ will have its center of mass displaced in proportion to uv . The position operator should therefore be of the form

$$\hat{x}_e = a_e (\hat{d}^\dagger \hat{p} + \hat{p}^\dagger \hat{d}), \quad (\text{B7})$$

where a_e is a length scale that we will obtain later from considerations of the optical sum-rule for the p - d transition. The velocity operator then follows from the Heisenberg equation of motion,

$$\hat{x}_e = \frac{i}{\hbar} [\hat{H}_e, \hat{x}_e] = ia_e \omega_e (\hat{d}^\dagger \hat{p} - \hat{p}^\dagger \hat{d}), \quad (\text{B8})$$

where for the sake of brevity we introduced the definition

$$\omega_e \equiv \frac{\epsilon_d - \epsilon_p}{\hbar}, \quad (\text{B9})$$

and we define the zero of energy such that $\epsilon_p = -\epsilon_d$. Applying the Heisenberg equation of motion a second time provides the result that the position operator satisfies the differential equation of a harmonic oscillator,

$$\hat{x}_e = \frac{i}{\hbar} [\hat{H}_e, \hat{x}_e] = -\omega_e^2 \hat{x}_e. \quad (\text{B10})$$

For later use it is useful to work out the commutator of the position and the velocity operator. By means of straightforward operator algebra we obtain

$$[\hat{x}_e, \hat{x}_e] = -\frac{4ia_e^2}{\hbar} \hat{H}_e. \quad (\text{B11})$$

To continue beyond this point we need to specify the ground state to which we are going to apply these rules. Here, we consider the case that the d state is empty, and the p state is occupied, i.e., $\langle \hat{d}^\dagger \hat{d} \rangle = 0$ and $\langle \hat{p}^\dagger \hat{p} \rangle = N_{p,e}$, then

$$\langle \hat{H}_e \rangle = -N_{p,e} \frac{\hbar \omega_e}{2}, \quad (\text{B12})$$

so that

$$\langle [\hat{x}_e, \hat{x}_e] \rangle = 2ia_e^2 \omega_e N_{p,e}. \quad (\text{B13})$$

Using the velocity and position operators introduced above, the f -sum rule following from linear response theory of the optical conductivity reads

$$\int_0^\infty \sigma_1(\omega) d\omega = \frac{\pi q_e^2}{2\hbar V} \text{Im} \langle [\hat{x}_e, \hat{x}_e] \rangle. \quad (\text{B14})$$

After substitution of the result of the commutator of Eq. (B13) we arrive at

$$\int_0^\infty \sigma_1(\omega) d\omega = \frac{\pi n_{p,e} q_e^2 a_e^2 \omega_e}{\hbar} = \frac{\pi n_{p,e} q_e^2}{2\tilde{m}_e}, \quad (\text{B15})$$

where $n_{p,e}$ is the volume density of the p electrons (i.e., the number of electrons in the $2p$ shell coupled to the Ti atom divided by the cell volume V). The right-hand member of the equation resembling the expression for the free-electron Drude spectral weight constitutes in fact the *definition* of the effective mass \tilde{m}_e of the electrons excited in the p - d transition. While in the present case the numbers work out to provide a mass value close to that of a free electron, the value of \tilde{m}_e employed in the analysis of the present model has to be taken from Eq. (B15) in the interest of internal consistency of the formalism.

Integration of $\sigma_1(\omega)/\omega^2$ provides another useful quantity, the static dielectric permittivity,

$$\int_0^\infty \frac{\sigma_1(\omega)}{\omega^2} d\omega = \frac{\epsilon(0) - 1}{8} = \frac{S_e}{8} = \frac{\pi n_{p,e} q_e^2 a_e^2}{\hbar \omega_e}. \quad (\text{B16})$$

The leftmost equality is a consequence of the Kramers-Kronig relation between the dissipative and dispersive components of the dielectric function. The last expression on the right is specific to the present model, and is a consequence of $\sigma_1(\omega)$ being proportional to $\delta(\omega - \omega_e)$.

By comparing the different members of the two expressions provided above, we see that the characteristic length scale a_e can be expressed either as a function of \tilde{m}_e or as a function of S ,

$$a_e = \sqrt{\frac{\hbar}{2\tilde{m}_e \omega_e}} = \sqrt{\frac{\hbar \omega_e S_e}{\pi n_{p,e} q_e^2}}. \quad (\text{B17})$$

Comparing the two right-hand members of the above equation, we see that the effective mass for the p - d transition is provided by the expression

$$\tilde{m}_e \equiv \frac{4\pi n_{p,e} q_e^2}{S_e \omega_e^2}. \quad (\text{B18})$$

Since we wish to extract parameters from optical data using a Lorentz-oscillator model both for the vibrational and electronic component, we use for this part of the analysis a boson representation of the electronic degree of freedom,

$$\begin{aligned} \hat{b}^\dagger &= \hat{d}^\dagger \hat{p}, & \hat{b} &= \hat{p}^\dagger \hat{d}, \\ \hat{x}_e &= a_e (\hat{b} + \hat{b}^\dagger), & \hat{p}_e &= \frac{\hbar}{2ia_e} (\hat{b} - \hat{b}^\dagger). \end{aligned} \quad (\text{B19})$$

It is important to note that the \hat{b} operators do not satisfy Bose-commutation rules. They do, however, provide a correct representation of the system provided that we restrict the states of the system to zero or one boson. In this limited sense we can map the electronic subsystem on a harmonic oscillator. The normal modes of the coupled system can be obtained by diagonalization of the coupled electronic-vibrational Hamiltonian in the classical limit. Using the above definitions of the electronic coordinates together with the vibrational coordinates, we obtain the Hamiltonian

$$\begin{aligned} H &= \frac{p_e^2}{2\tilde{m}_e} + \frac{\tilde{m}_e \omega_e^2}{2} x_e^2 + \frac{p_n^2}{2m_n} + \frac{m_n \omega_n^2}{2} x_n^2 \\ &+ E(q_e x_e + q_n x_n) - \gamma x_e x_n, \end{aligned} \quad (\text{B20})$$

where γ is the spring constant connecting the electronic and vibrational degrees of freedom. In the interest of compactness

we have absorbed all terms proportional to x_e^2 and x_n^2 in the definitions of ω_e and ω_n . For a harmonic time-varying electric field with angular frequency ω , the nuclear and electronic currents are

$$j_n = i\omega x_n q_n n_n, \quad j_e = i\omega x_e q_e n_e, \quad (\text{B21})$$

and the coupled classical equations of motion become

$$\begin{bmatrix} \tilde{m}_e(\omega^2 - \omega_e^2) & \gamma \\ \gamma & m_n(\omega^2 - \omega_n^2) \end{bmatrix} \begin{pmatrix} x_e \\ x_n \end{pmatrix} = \begin{pmatrix} q_e E \\ q_n E \end{pmatrix}. \quad (\text{B22})$$

The solution for the vibrational conductivity $\sigma_n = j_n/E$ is

$$\sigma_n(\omega) = \frac{q_n^2 n_n}{m_n} \frac{i\omega Z_{\text{eff}}^2(\omega)}{\omega^2 - \tilde{\omega}_n^2(\omega)}. \quad (\text{B23})$$

Due to the electron-phonon coupling the vibrational frequency has shifted to

$$\tilde{\omega}_n^2(\omega) = \omega_n^2 - \frac{\gamma^2 m_n^{-1} \tilde{m}_e^{-1}}{\omega_e^2 - \omega^2}. \quad (\text{B24})$$

The transverse effective charge is given by

$$Z_{\text{eff}}^2(\omega) = 1 + \frac{\gamma \tilde{m}_e^{-1}}{\omega_e^2 - \omega^2}. \quad (\text{B25})$$

In the case of SrTiO₃ the electronic and vibrational frequencies are separated by two orders of magnitude. Consequently, for the range of vibrational frequencies, this expression can be

used in the limit $\omega \rightarrow 0$. The coupling constant γ is readily obtained from the transverse effective charge through the relation

$$\gamma = (Z_{\text{eff}}^2 - 1) \tilde{m}_e \omega_e^2 = (Z_{\text{eff}}^2 - 1) \frac{4\pi n_{p,e} q_e^2}{S_e}. \quad (\text{B26})$$

Once we have read out Z_{eff} , S_e , ω_e , ω_n , and γ from the optical data, we are ready to set up the observables on the quantum level. The nuclear position and momentum operators are

$$\hat{x}_n = a_n(\hat{a} + \hat{a}^\dagger), \quad \hat{p}_n = \frac{\hbar}{2ia_n}(\hat{a} - \hat{a}^\dagger), \quad (\text{B27})$$

where the characteristic length scale is given by

$$a_n = \sqrt{\frac{\hbar}{2m_n\omega_n}}. \quad (\text{B28})$$

The Hamiltonian operator of the coupled electron-phonon system is

$$\begin{aligned} \hat{H} = & \frac{\hbar\omega_e}{2}(\hat{d}^\dagger \hat{d} - \hat{p}^\dagger \hat{p}) + \hbar\omega_n \left(\frac{1}{2} + \hat{a}^\dagger \hat{a} \right) \\ & - g(\hat{d}^\dagger \hat{p} + \hat{p}^\dagger \hat{d})(\hat{a}^\dagger + \hat{a}). \end{aligned} \quad (\text{B29})$$

The constant g is the spring constant connecting the electron and nuclear oscillator, multiplied by the characteristic length of the electronic oscillator and the nuclear one,

$$g \equiv \gamma a_n a_e. \quad (\text{B30})$$

-
- [1] J. F. Schooley, W. R. Hosler, and M. L. Cohen, *Phys. Rev. Lett.* **12**, 474 (1964).
[2] C. S. Koonce, M. L. Cohen, J. F. Schooley, W. R. Hosler, and E. R. Pfeiffer, *Phys. Rev.* **163**, 380 (1967).
[3] J. G. Bednorz and K. A. Müller, *Rev. Mod. Phys.* **60**, 585 (1988).
[4] X. Lin, Z. Zhu, B. Fauqué, and K. Behnia, *Phys. Rev. X* **3**, 021002 (2013).
[5] C. Collignon, X. Lin, C. W. Rischau, B. Fauqué, and K. Behnia, *Annu. Rev. Condens. Matter Phys.* **10**, 25 (2019).
[6] K. A. Müller and H. Burkard, *Phys. Rev. B* **19**, 3593 (1979).
[7] M. Itoh, R. Wang, Y. Inaguma, T. Yamaguchi, Y.-J. Shan, and T. Nakamura, *Phys. Rev. Lett.* **82**, 3540 (1999).
[8] S. E. Rowley, L. J. Spalek, R. P. Smith, M. P. M. Dean, M. Itoh, J. F. Scott, G. G. Lonzarich, and S. S. Saxena, *Nat. Phys.* **10**, 367 (2014).
[9] A. Stucky, G. W. Scheerer, Z. Ren, D. Jaccard, J.-M. Pomirol, C. Barreateau, E. Giannini, and D. van der Marel, *Sci. Rep.* **6**, 37582 (2016).
[10] C. W. Rischau, X. Lin, C. P. Grams, D. Finck, S. Harms, J. Engelmayer, T. Lorenz, Y. Gallais, B. Fauqué, J. Hemberger, and K. Behnia, *Nat. Phys.* **13**, 643 (2017).
[11] Y. Tomioka, N. Shirakawa, K. Shibuya, and I. H. Inoue, *Nat. Commun.* **10**, 738 (2019).
[12] M. L. Cohen, *Phys. Rev.* **134**, A511 (1964).
[13] D. M. Eagles, *Phys. Rev.* **186**, 456 (1969).
[14] J. Appel, *Phys. Rev.* **180**, 508 (1969).
[15] Z. Zinamon, *Philos. Mag.* **21**, 347 (1970).
[16] K. L. Ngai, *Phys. Rev. Lett.* **32**, 215 (1974).
[17] T. Jarlborg, *Phys. Rev. B* **61**, 9887 (2000).
[18] D. van der Marel, J. L. M. van Mechelen, and I. I. Mazin, *Phys. Rev. B* **84**, 205111 (2011).
[19] S. N. Klimin, J. Tempere, D. van der Marel, and J. T. Devreese, *Phys. Rev. B* **86**, 045113 (2012).
[20] J. M. Edge, Y. Kedem, U. Aschauer, N. A. Spaldin, and A. V. Balatsky, *Phys. Rev. Lett.* **115**, 247002 (2015).
[21] L. P. Gor'kov, *Proc. Natl. Acad. Sci. USA* **113**, 4646 (2016).
[22] J. Ruhman and P. A. Lee, *Phys. Rev. B* **94**, 224515 (2016).
[23] Y. Kedem, J.-X. Zhu, and A. V. Balatsky, *Phys. Rev. B* **93**, 184507 (2016).
[24] Y. Kedem, *Phys. Rev. B* **98**, 220505(R) (2018).
[25] P. Wölfle and A. V. Balatsky, *Phys. Rev. B* **98**, 104505 (2018).
[26] S. E. Rowley, C. Enderlein, J. F. de Oliveira, D. A. Tompsett, E. Baggio Saitovitch, S. S. Saxena, and G. G. Lonzarich, [arXiv:1801.08121](https://arxiv.org/abs/1801.08121).
[27] J. Ruhman and P. A. Lee, [arXiv:1901.11065](https://arxiv.org/abs/1901.11065).
[28] J. T. Devreese, S. N. Klimin, J. L. M. van Mechelen, and D. van der Marel, *Phys. Rev. B* **81**, 125119 (2010).
[29] W. Meevasana, X. J. Zhou, B. Moritz, C.-C. Chen, R. H. He, S.-I. Fujimori, D. H. Lu, S.-K. Mo, R. G. Moore, F. Baumberger, T. P. Devereaux, D. van der Marel, N. Nagaosa, J. Zaanen, and Z.-X. Shen, *New J. Phys.* **12**, 023004 (2010).
[30] M. N. Gastiasoro, A. V. Chubukov, and R. M. Fernandes, *Phys. Rev. B* **99**, 094524 (2019).
[31] W. Zhong, R. D. King-Smith, and D. Vanderbilt, *Phys. Rev. Lett.* **72**, 3618 (1994).

- [32] D. van der Marel, in *Quantum Materials: Experiments and Theory*, edited by E. Pavarini, E. Koch, J. van den Brink, and G. Sawatzky, Lecture Notes of the Autumn School on Correlated Electrons 2016, Modeling and Simulation Vol. 6 (Forschungszentrum Jülich, Jülich, 2016), Chap. 11.
- [33] M. J. Rice, N. O. Lipari, and S. Strässler, *Phys. Rev. Lett.* **39**, 1359 (1977).
- [34] M. J. Rice and H.-Y. Choi, *Phys. Rev. B* **45**, 10173 (1992).
- [35] A. Damascelli, K. Schulte, D. van der Marel, and A. A. Menovsky, *Phys. Rev. B* **55**, R4863 (1997).
- [36] E. Cappelluti, L. Benfatto, M. Manzardo, and A. B. Kuzmenko, *Phys. Rev. B* **86**, 115439 (2012).
- [37] A. H. Kahn and A. J. Leyendecker, *Phys. Rev.* **135**, A1321 (1964).
- [38] M. Cardona, *Phys. Rev.* **140**, A651 (1965).
- [39] T. C. Asmara, A. Annadi, I. Santoso, P. K. Gogoi, A. Kotlov, H. M. Omer, M. Motapothula, M. B. H. Breese, M. Rübhausen, T. Venkatesan, Ariando, and A. Rusydi, *Nat. Commun.* **5**, 3663 (2014).
- [40] We thank an anonymous referee for drawing our attention to this.
- [41] Since the dispersion measured by Stirling [42] is only provided along a limited set of high-symmetry directions in momentum space, we approximate the momentum dependence by $\omega_q = \sqrt{\omega_{\text{TO1}}^2 + \omega_{\text{ZB}}^2 \sin^2(qa/2)}$ in a three-dimensional Brillouin sphere of radius $q = \pi/a$. For optimal doping ($n = 10^{20} \text{ cm}^{-3}$) the frequency of the TO1 mode is $\hbar\omega_{\text{TO}} = 6 \text{ meV}$ [46]. Stirling [42] reported for the TO1 branch a frequency of 3 THz at the Brillouin-zone boundary. In the limit of a small Fermi momentum we can use the approximation $q' \approx -q$, so that $\omega_{q'} \approx \omega_q$. With these parameters the numerical evaluation of $1/2\omega_n = \langle 1/(\omega_q + \omega_{q'}) \rangle$ yields $2\hbar\omega_n = 24 \text{ meV}$.
- [42] W. G. Stirling, *J. Phys. C: Solid State Phys.* **5**, 2711 (1972).
- [43] U. Aschauer and N. A. Spaldin, *J. Phys.: Condens. Matter* **26**, 122203 (2014).
- [44] J. L. Servoin, Y. Luspin, and F. Gervais, *Phys. Rev. B* **22**, 5501 (1980).
- [45] K. Kamaras, K.-L. Barth, F. Keilmann, R. Henn, M. Reedyk, C. Thomsen, M. Cardona, J. Kircher, P. L. Richards, and J.-L. Stehle, *J. Appl. Phys.* **78**, 1235 (1995).
- [46] J. L. M. van Mechelen, D. van der Marel, C. Grimaldi, A. B. Kuzmenko, N. P. Armitage, N. Reyren, H. Hagemann, and I. I. Mazin, *Phys. Rev. Lett.* **100**, 226403 (2008).
- [47] H. Fröhlich, *Adv. Phys.* **3**, 325 (1954).
- [48] Y. Toyozawa, *Polarons in Ionic Crystals and Polar Semiconductors* (North-Holland, Amsterdam, 1972), pp. 1–27.
- Correction:* Minor errors in a factor in the numerator of Eq. (7) and in the value for the radius given in Ref. [41] have been fixed.